Article

Heartbeat-Induced Corneal Axial Displacement and Strain Measured by High Frequency Ultrasound Elastography in Human Volunteers

Sunny Kwok[1], Keyton Clayson[1,2], Nicholas Hazen[1,2], Xueliang Pan[3], Yanhui Ma[1,4], Andrew J. Hendershot[4], and Jun Liu[1,2,4]

[1] Department of Biomedical Engineering, The Ohio State University, Columbus, OH, USA
[2] Biophysics Interdisciplinary Group, The Ohio State University, Columbus, OH, USA
[3] Department of Biomedical Informatics, The Ohio State University, Columbus, OH, USA
[4] Department of Ophthalmology and Visual Science, The Ohio State University, Columbus, OH, USA

Purpose: The purpose of this study was to establish in vivo data acquisition and processing protocols for repeatable measurements of heartbeat-induced corneal displacements and strains in human eyes, using a high-frequency ultrasound elastography method, termed ocular pulse elastography (OPE).

Methods: Twenty-four volunteers with no known ocular diseases were recruited for this study. Intraocular pressure (IOP) and ocular pulse amplitude (OPA) were measured using a PASCAL Dynamic Contour Tonometer (DCT). An in vivo OPE protocol was developed to measure heartbeat-induced corneal displacements. Videos of the central 5.7 mm of the cornea were acquired using a 50-MHz ultrasound probe at 128 frames per second. The radiofrequency data of 1000 frames were analyzed using an ultrasound speckle tracking algorithm to calculate corneal displacements and quantify spectral and temporal characteristics. The intrasession and intersession repeatability of OPE- and DCT-measured parameters were also analyzed.

Results: The in vivo OPE protocol and setup were successful in tracking heartbeat-induced corneal motion using high-frequency ultrasound. Corneal axial displacements showed a strong cardiac rhythm, with good intrasession and intersession repeatability, and high interocular symmetry. Corneal strain was calculated in two eyes of two subjects, showing substantially different responses.

Conclusions: We demonstrated the feasibility of high-frequency ultrasound elastography for noninvasive in vivo measurement of the cornea's biomechanical responses to the intrinsic ocular pulse. The high intrasession and intersession repeatability suggested a robust implementation of this technique to the in vivo setting.

Translational Relevance: OPE may offer a useful tool for clinical biomechanical evaluation of the cornea by quantifying its response to the intrinsic pulsation.

Introduction

At each heartbeat, the pulsatile ocular blood flow induces a transient change of the intraocular volume and thus creates an ocular pulse, a fluctuation of the intraocular pressure (IOP) above its diastolic level. The average ocular pulse amplitude (OPA) is about 3 mm Hg in humans.[1] This ocular pulse produces an expansion of the cornea, which is dependent on the IOP and OPA, as well as the biomechanical properties of the cornea. Using ex vivo porcine and human donor globes with simulated ocular pulse superimposed on a baseline IOP, we have shown that high-frequency ultrasound elastography (termed the ocular pulse elastography [OPE]) can reliably detect corneal axial displacement and strain induced by simulated ocular pulses with high sensitivity and accuracy.[2,3] These results

suggest that the OPE technique may provide an in vivo tool for evaluating corneal biomechanical responses and properties.

Translating the OPE technique to the in vivo setting presents several challenges. In our ex vivo experiments, the donor globes were immersed in liquid, which provides acoustic coupling between the ultrasound probe and the cornea.[3] A new acoustic coupling mechanism is needed for convenient and reproducible in vivo measurements. The ex vivo measurement apparatus, including the probe, the specimen, and the specimen holder, was placed on an antivibration table to shield the system from environmental motion noise and ensure precise displacement measurements. An in vivo experimental setup needs to be similarly designed to minimize environmental motion noise, such as building vibrations. Another challenge is the presence of various physiological motions in vivo. Involuntary eye motion, including microsaccades, tremor, and drift,[4] or other forces acting on the cornea could introduce artefacts and potentially lead to unsatisfactory or even loss of tracking of the imaging plane. In addition, heartbeat or breathing-induced head/whole globe motion could be significant and difficult to separate from corneal expansion.[5]

In this study, we developed new data acquisition protocols to measure human corneas in vivo using high-frequency ultrasound. We also developed data processing methods to quantify heartbeat-induced corneal axial motion in the presence of physiological motion noise. The high-frequency ultrasound elastography approach has several advantages as a potential tool for in vivo characterization of corneal biomechanics. First, high-frequency ultrasound at 50 MHz can sufficiently penetrate the entire thickness of the human cornea and generate strong speckle signals for speckle tracking. We have implemented a method to densely sample the radiofrequency (RF) data, which are voltage values of the ultrasound signals, to achieve very high displacement sensitivity reaching 10s of nanometers with interpolation.[2,6] Second, the OPE technique tracks displacements of many spatial points within the scanned corneal cross-section. Local mechanical strains can be computed from the spatial gradients of the displacements, which may be distinct in ocular diseases, such as keratoconus and glaucoma. Microstructure analyses[7] and ex vivo testing[8] have suggested mechanical weakening in keratoconic corneas, whereas corneal biomechanical properties have also been linked to glaucoma damage[9] and IOP spikes.[10] Third, ultrasound has a high temporal resolution, which permits dense temporal sampling to ensure capturing the dynamics responses and successful tracking in the presence of physiological motion. Fourth, the 2D cross-sectional ultrasound images also provide information of corneal geometry, including thickness and curvature. These data can be combined with the biomechanical data from speckle tracking to build computational models and derive eye-specific tissue properties. In this study, a 50-MHz ultrasound imaging system was used to capture videos of the central 5.7 mm of the cornea and acquire both images and RF data at 128 frames per second while the eye was fixated on a distant target. The RF data were analyzed to evaluate the temporal and spectral characteristics of corneal axial displacements in human volunteers with no known corneal diseases. Intra- and intersession repeatability of the OPE measurements was evaluated. Calculations of corneal axial strain were also demonstrated in two eyes with similar OPA and diastolic IOP. These studies aimed to demonstrate the feasibility of OPE as an in vivo tool to characterize corneal motion and strain, which may provide useful evaluations of corneal biomechanical properties for better diagnosis and improved understanding of ocular diseases, such as keratoconus and glaucoma.[11–14]

Methods

Participants

This study was conducted with informed written consent of all participants, in adherence to the tenets of the Declaration of Helsinki and with approval of The Ohio State University Institutional Review Board. Twenty-four subjects with no known corneal pathology or surgeries were enrolled (age = 21–72 years old; 9 men and 15 women). To assess intersession (between visits) repeatability, a subset of subjects ($n = 9$ subjects, 18 eyes) was invited to complete a second visit 6 to 10 months later after the first visit.

Measurement Setup and Testing Protocols

Each subject underwent three tests at each visit, in the order described below:

1) Corneal topography was first acquired in both eyes of the subject using a Keratron Scout with a near Mires cone (Optikon, Inc., Rome, Italy) to confirm a normal corneal topography. Three repeated measurements were obtained in each eye.
2) Dynamic IOP over several cardiac cycles was measured using the PASCAL Dynamic Contour Tonometer (DCT; Ziemer USA, Alton, IL).
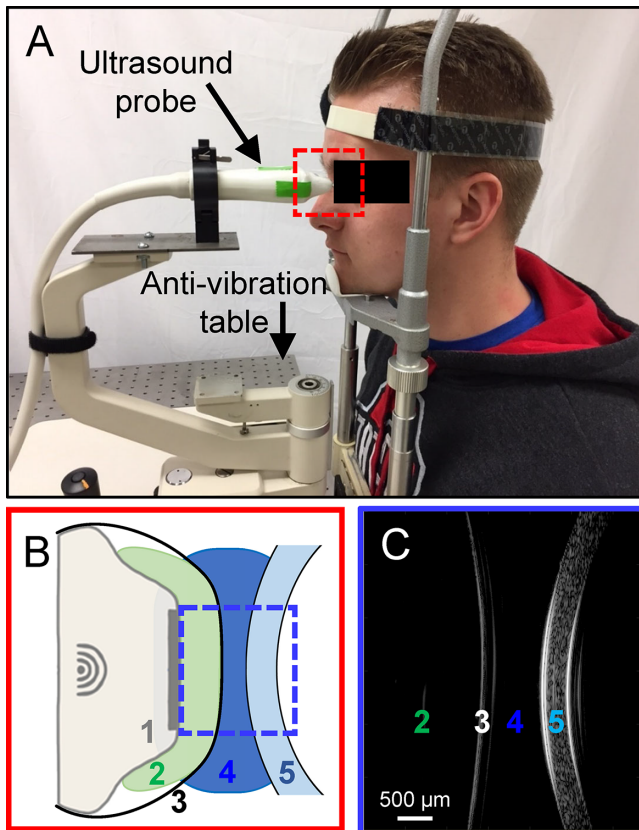
Figure 1. (**A**) In vivo OPE setup: a subject sits in front of an antivibration table with the head strapped into the chin-and-forehead rest mounted on the table. The ultrasound probe is mounted on a holder whose position can be adjusted by an operator. (**B**) A close-up of the probe tip and the cornea during ultrasound scanning: 1. ultrasound probe, 2. alginate gel, 3. ClearScan probe cover, 4. GenTeal gel, and 5. subject cornea. Items 2 to 4 transmit ultrasound signals with minimal acoustic attenuation. (**C**) Ultrasound B-mode image of 2 through 5 in **B**.

FUJIFilm VisualSonics, Inc., Toronto, Canada) was secured to a probe-holder mounted on the antivibration table. An acoustic coupling system was designed to efficiently transmit acoustic waves between the ultrasound transducer and the eye. Specifically, a sterile cellulose membrane (ClearScan CS2000; ESI, Inc., Plymouth, MN) was placed over the transducer head, enclosing a layer of solidified sodium alginate gel about 3 mm thick. A layer of eye lubricating gel (GenTeal Severe Dry Eye Relief or Systane Nighttime Protection, Alcon, Inc., Ft. Worth, TX) was placed on the exterior of the probe cover (see Fig. 1B). The alginate gel, the cellulose membrane, and the eye lubricating gel are all translucent to ultrasound, which ensures an efficient transduction of acoustic energy between the probe and the eye. These items were disposed of and reapplied after each patient use.

Anesthetic eye drops (Tetracaine HCl 0.5%; Bausch & Lomb, Bridgewater, NJ) were applied to both eyes prior to measurements. The subject's head was secured to the head-and-chin rest with a tight head strap to minimize head motion. The nonmeasured eye was fixated at a distant target while both eyes were open. The position of the probe was adjusted by an operator to align the scanning plane to the horizontal cross-section along the nasal-temporal meridian of the cornea. The ultrasound probe was then advanced toward the eye until the gel layer established contact with the cornea and the corneal image started to appear on the monitor screen. The operator further fine-tuned the probe position based on the cornea's live image on the monitor screen to ensure that the cornea was centered in the image and positioned within the focal zone of the scan (see Fig. 1C). One thousand consecutive B-mode frames and RF data of the central 5.7 mm of cornea were then acquired at 128 frames per second. Three repeated measurements were obtained in each eye, with additional gel applied to the probe exterior as needed. The right eye (OD) was measured first, followed by the left eye (OS) in all subjects. In a subset of subjects ($n = 10$), an electrocardiogram (ECG; MP36; BIOPAC, Goleta, CA) was simultaneously recorded by attaching the limb leads to the subject's left arm, right arm, and right leg.

Three repeated measurements were obtained in each eye. DCT outputs, including the diastolic IOP, OPA, and heart rate (HR_{DCT}), were recorded.

3) Dynamic corneal motion was measured using the OPE technique. Three repeated measurements were recorded in each eye and the signals were further processed to obtain the corneal axial displacement (CAD), heart rate (HR_{OPE}), and central corneal thickness (CCT). The details are described below.

To minimize vertical environmental motion noise and head motion, the subject sat at an antivibration table (ScienceDesk Workstations; Thorlabs, Newton, NJ) with the head placed in a heavy-duty head-and-chin rest mounted on the table (Fig. 1A). An ultrasound probe (50 MHz, MS700, Vevo 2100,

Corneal Displacements Calculated from Ultrasound Speckle Tracking

Corneal displacements were calculated using an ultrasound speckle tracking algorithm described and validated previously.[2,3,15,16] Briefly, the RF data were

acquired and stored as 300 A-lines spaced at 19 µm intervals. Each A-line was sampled at approximately 1.5 µm intervals. Speckle tracking was performed on RF data. A region of interest (ROI) was defined in the reference frame (i.e. first acquired frame) of the RF data by automatic segmentation of the corneal stroma using MatLab version 2020a (The Math Works, Inc., Natick, MA) functions (*findpeaks*, Signal Processing Toolbox; *edge*, Image Processing Toolbox), based on the high acoustic signals from the anterior and posterior surfaces of the central cornea. The resulting ROI was approximately 4 mm in width. About 200 grid points spaced by 13 × 10 pixels (axial × lateral), or approximately 19.5 µm × 190 µm, were defined within the ROI. Kernels centered at each grid point containing 51 × 41 pixels were defined.[2,3] To compute the displacement at each grid point, the unique speckle pattern within its surrounding kernel was tracked in subsequent frames using cross-correlation. The maximum correlation coefficient value indicated the best match and the corresponding kernel center was designated as the new location of the displaced grid point. Spline interpolation was used for subpixel tracking. To reduce processing time, we down-sampled the 1000 scanned frames by a factor of 5 and calculated displacements between down-sampled frames (200 in total). The displacement vector of each grid point was obtained between two consecutively sampled frames and accumulated over all 200 frames. Because the accuracy of axial displacement was much higher than that of lateral displacement due to higher spatial resolution and sampling density,[2] only axial displacements were used for further analysis, although lateral displacements were also calculated. The average axial displacement of all grid points within the ROI was plotted as the cumulative corneal axial displacement (cCAD) curve.

The cCAD signal was filtered to remove noise using a band-pass filter. The heart rate frequency (F_{HR}) for each dataset was first identified automatically as the strongest peak in the frequency spectrum within the physiological range corresponding to a heart rate (HR) of 50 to 100 beats-per-minute. Frequency components below $\frac{1}{2}F_{HR}$, above $3F_{HR}$, and those with magnitudes below 10% of the maximum peak were removed.[17] The frequency spectra of dynamic IOP (as measured by DCT), ECG, and cCAD were compared. The heart rate derived from cCAD (HR_{OPE}) was compared with those obtained from DCT (HR_{DCT}) in 23 subjects (one subject did not yield satisfactory DCT data). The HR derived from cCAD was also compared with the HR from simultaneously measured ECG in 10 subjects (HR_{ECG}).

Among the three OPE measurements, one of the measurements in some eyes (often the first attempt in a given eye) did not yield satisfactory data (i.e. no discernable cycles were observed in band-pass filtered cCAD). B-mode videos revealed excessive eye motion during these measurements. In one eye, only one of the measurements was void of excessive eye motion. For each satisfactory OPE measurement, CAD was calculated as the average trough-to-peak magnitudes of three displacement cycles (Fig. 2) that were automatically identified. Troughs were first identified as local minima, and the corresponding peak was identified as the maxima between two consecutive troughs no less than one fifth of the HR distance from the first trough. Two repeated measurements during one visit (6 trough-to-peak amplitudes in total) were used to obtain the average CAD of an eye for that visit.

Central Cornea Thickness

Although the Vevo2100 system has built-in software for measuring the distance between two selected points which can be used to obtain tissue thickness, we developed an automated algorithm to reduce ambiguity from manual selection of boundary points. The algorithm identified the anterior and posterior cornea surfaces based on RF signal intensity in the 500th B-mode frame, which was the RF frame obtained at the mid-point of data acquisition during each measurement. MatLab version 2020a (The Math Works, Inc.) functions *findpeaks* (Signal Processing Toolbox) and *edge* (Image Processing Toolbox) were applied to the RF data following a similar procedure for identifying ROI. The smallest corneal thickness of all scanned A-lines on this frame was recorded as the CCT.

Corneal Strain Estimation

The spatial gradient of corneal displacements was analyzed in two subjects measured on the same day to evaluate feasibility of measuring in vivo corneal strains induced by ocular pulse. For each subject, B-mode frames corresponding to the local trough and peak of a representative displacement cycle were identified from the filtered cCAD curves, and CAD between these two frames at each defined grid point was calculated using the ultrasound speckle tracking algorithm between these two frames. The corneal axial strain (CAS) at each grid point was calculated using a least squares strain estimation technique[16,18] based on the local gradient of displacements. The strains were smoothed by a 7 × 7 mean-filter (gradually adapted to 5 × 5 or 3 × 3 for more boundary kernels). Strain maps were then generated with spline interpolation to the pixel level.
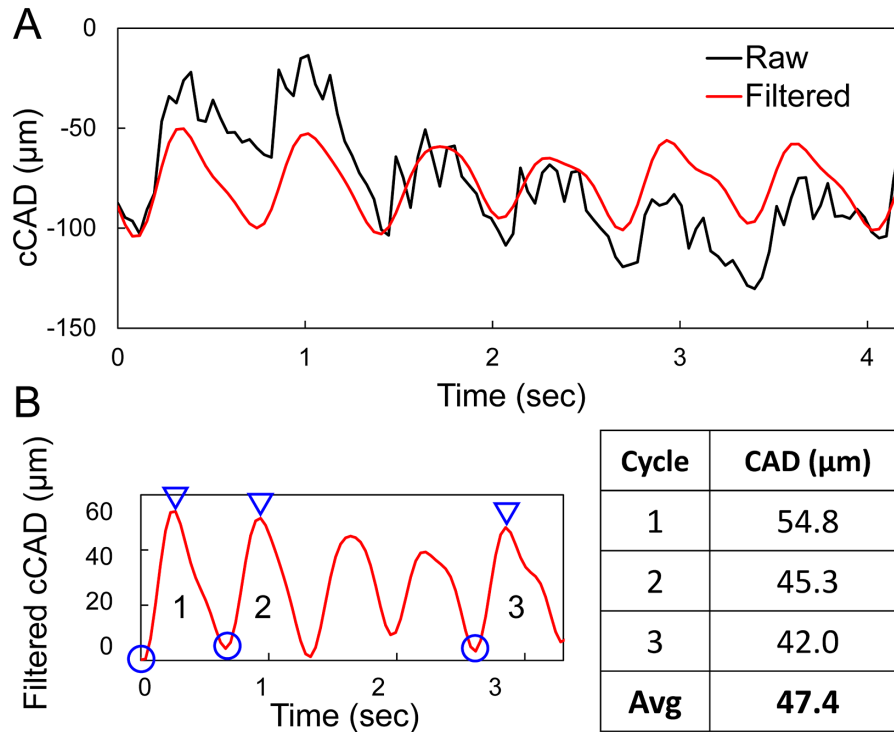
Figure 2. (**A**) Raw (*black*) and band-pass filtered (*red*) cCAD of one measurement in a subject (**B**) CAD for each measurement was calculated as the average trough (*circle*)-to-peak (*triangle*) magnitudes for three automatically selected cycles.

Statistical Analysis and Intra- and Intersession Repeatability

For each eye, we recorded up to three values of the CAD, CCT, and HR_{OPE} obtained from the OPE measurements, as well as three values of the IOP, OPA, and HR_{DCT} from the DCT measurements. The average of these repeated measures for each eye was used to generate the summary statistics (using mean and standard deviations) for all 24 participants.

The repeatability of the OPE measurements of CAD, CCT, and HR_{OPE} were evaluated using the scatter plots, the Bland-Altman plots, and the Intra-class Correlation Coefficients (ICC) of the single measure of two to three repeated measures based on the Shrout and Fleiss convention.[19] ICC ranges from 0 to 1, with 0 indicating poor agreement and 1 for perfect agreement. The Cicchetti's guideline suggests ICC < 0.40 as poor, 0.40 to 0.60 as fair, 0.60 to 0.75 as good, and > 0.75 as excellent agreement.[20] ICCs were also used to evaluate the repeatability of diastolic IOP, OPA, and HR_{DCT} from three repeated DCT measurements during one visit.

Similar methods were used to evaluate the intersession repeatability of both OPE and DCT measurements in 18 eyes of the 9 subjects that completed 2 visits.

Correlations among CAD and IOP, OPA, CCT, or age were explored using Pearson correlation.

Results

Keratron readings were reviewed by a corneal specialist and confirmed the absence of ectasia or abnormal topography in all enrolled subjects. DCT measurements (mean diastolic IOP, OPA, and HR_{DCT}) and OPE measurements (CAD, CCT, and HR_{OPE}) are summarized in Table 1.

The raw cCAD contained both cyclic and abrupt changes in the measured eyes. The abrupt changes in cCAD were related to microsaccades, as confirmed by B-mode videos (see Supplementary Video S1). Figure 3 shows an example of one measurement with cumulative axial and lateral displacements (cCAD and cCLD) and speckle-tracking correlation coefficients over time. The correlation coefficients between consecutive frames were very high (over 0.95) throughout the recordings, except at time points corresponding to microsaccades (see Fig. 3). Most microsaccades involved both axial and lateral motion of the eye and were indicated in both the cCAD and the cCLD curves (see Fig. 3). Slow drifts were observed frequently in

Table 1. Summary of OPE and DCT Measurements in 24 Subjects

OPE	Mean ± SD	Range
CAD, µm		
OD, $n = 23$	47.1 ± 17.6	[17.9, 98.5]
OS, $n = 24$	47.1 ± 15.6	[18.2, 88.2]
CCT, µm		
OD, $n = 23$	526 ± 30	[467, 587]
OS, $n = 24$	528 ± 32	[464, 586]
HR_{OPE}, bpm		
OD, $n = 23$	70.2 ± 11.4	[54.3, 98.8]
OS, $n = 24$	70.5 ± 12.6	[40.6, 101]
DCT	**Mean ± SD**	**Range**
Diastolic IOP, mm Hg		
OD, $n = 23$	16.7 ± 2.8	[9.5, 22.5]
OS, $n = 24$	16.0 ± 2.4	[11.1, 22.1]
OPA, mm Hg		
OD, $n = 23$	2.6 ± 0.9	[0.9, 5.0]
OS, $n = 24$	2.4 ± 0.8	[0.8, 4.1]
HR_{DCT}, bpm		
OD, $n = 23$	74.2 ± 16.3	[48, 148]
OS, $n = 24$	70.2 ± 9.0	[53, 96]

Figure 3. The cumulative corneal axial and lateral displacements (cCAD and cCLD) and the corresponding speckle tracking correlation coefficient (Corr.) in one subject showing the effects of microsaccades (*short, solid arrows*) and drifts (*dashed arrows*). Speckle tracking correlation coefficients remained very high (close to 1.0) except at time points of microsaccades that affected both axial and lateral displacements. Drifts did not affect correlation coefficients.

most measured eyes, but did not induce noticeable reduction of correlation coefficients.

Frequency spectral plots showed that the first two harmonics were at similar frequencies between asynchronously measured IOP and cCAD (Figs. 4A, 4B) and almost identical frequencies between synchronously measured ECG and cCAD (Figs. 4C, 4D). In addition, the HRs from OPE and DCT measurements were strongly correlated ($R = 0.96$, $P < 0.001$, $n = 23$; Fig. 5A). HRs from synchronously recorded ECG in 10 subjects showed an even stronger correlation with OPE-measured HRs in these subjects ($R = 0.99$, $P < 0.001$; see Fig. 5B).

The intrasession repeatability of OPE measurements is illustrated in Figure 6 and the ICCs are presented in Table 2. The two measurements of CAD and CCT during the same visit (corresponding to the two OPE measurements with satisfactory speckle tracking) were strongly correlated ($R = 0.80$ and 0.98, respectively; P values < 0.001; $n = 47$ eyes; see Fig. 6), with good or excellent agreement among all repeated measures (ICCs were 0.72 and 0.97, respectively; see Table 2). The two measurements of HR_{OPE} was also significantly correlated ($R = 0.56$, $P < 0.001$), but larger variability was observed in some eyes and the ICC was 0.53 (fair agreement). The ICCs for three repeated DCT measurements within one visit are also presented in Table 2. In the OD/OS combined analysis,
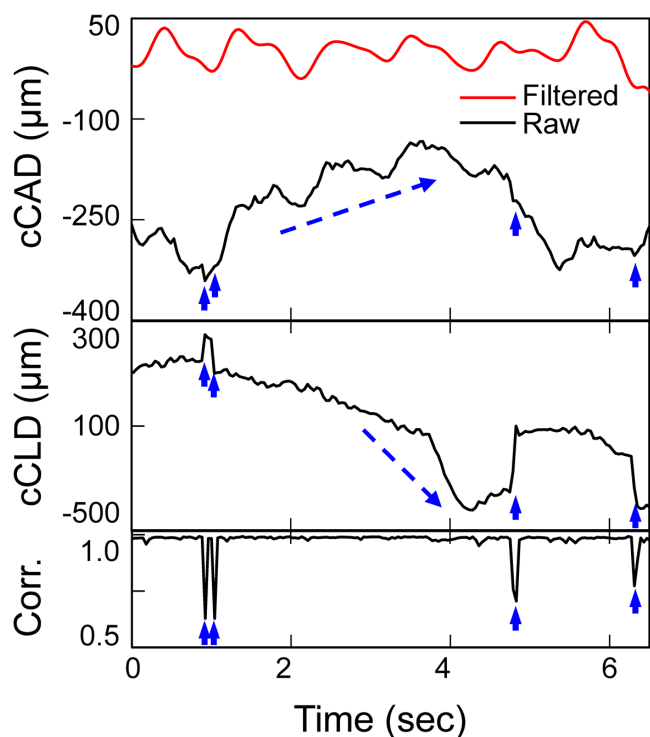
both diastolic IOP and OPA had ICCs greater than 0.6 showing good agreement, whereas the ICC for HR_{DCT} was lower (0.46; fair agreement).

The intersession repeatability of DCT measurements is shown in Table 2. Both diastolic IOP and OPA were significantly correlated between visits ($R = 0.65$ and 0.72, $P = 0.004$ and < 0.001, respectively, $n = 18$ eyes) with ICCs of 0.71 and 0.78 showing good and excellent agreement, respectively. HR_{DCT} was not correlated between visits ($R = 0.07$, $P = 0.78$, $n = 18$ eyes) and its ICC also showed poor agreement (0.26). The intersession repeatability of the OPE measurements is shown in Table 2 and Figure 7. CCT measured between the two visits was highly correlated ($R = 0.98$, $P < 0.001$, $n = 18$ eyes) and the ICC was 0.99 (excellent agreement). CAD was significantly correlated between visits ($R = 0.55$, $P = 0.02$, $n = 18$ eyes) with an ICC of 0.71 (good agreement). HR_{OPE} was not correlated between visits ($R = 0.11$, $p = 0.65$, $n = 18$ eyes), whereas the ICC indicated fair agreement (0.45).
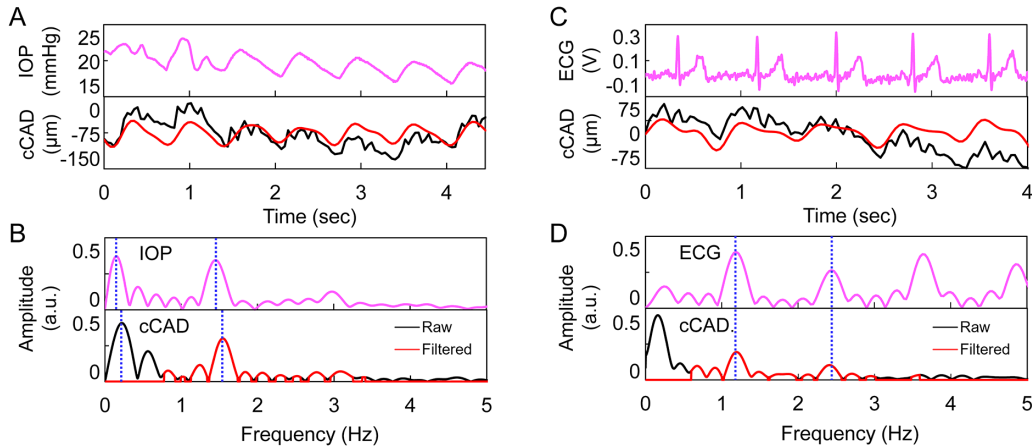
Figure 4. (**A, B**) Comparison of asynchronously recorded dynamic IOP and cCAD in one subject. (**A**) *Top*: dynamic IOP. *Bottom*: raw (*black*) and band-pass filtered (*red*) cCAD. (**B**). *Top*: frequency spectrum of dynamic IOP. *Bottom*: frequency spectrum of raw cCAD (*black*) overlaid with the filtered frequency spectrum (*red*). (**C, D**) Comparison of synchronously recorded ECG and cCAD in another subject. (**C**) *Top*: raw ECG signal. *Bottom*: raw (*black*) and band-pass filtered (*red*) cCAD. (**D**) *Top*: frequency spectrum of ECG. *Bottom*: frequency spectrum of raw cCAD (*black*) overlaid with the filtered frequency spectrum (*red*), where a constant offset was removed. The *dotted vertical lines* indicate the first two harmonics.

The intrasession and intersession repeatability were also analyzed in OD and OS separately, and the results were generally consistent with the combined analysis (see Table 2).

CAD was strongly correlated between OD and OS ($R = 0.79$, $P < 0.001$; Fig. 8). CCT, IOP, and OPA were also strongly correlated between the two eyes of the same subject ($R = 0.98, 0.77$, and 0.85, respectively, $P < 0.001$). In our explorative analysis, no significant correlation was found between CAD and other parameters including IOP, OPA, CCT, or age. Future studies are needed to re-evaluate potential correlations in a larger sample size.

Corneal Strain

CAS in two eyes of two subjects are shown in Figure 9. The diastolic IOP (19 and 17 mm Hg) and OPA (2.3 and 2.5 mm Hg) were similar between these two subjects. Both corneas showed negative strains indicating corneal thinning from the trough to the peak point of axial displacement. The CAS was -0.03% in subject 1 and 14 times larger in subject 2 (-0.42%), who had a thinner cornea (584 μm vs. 482 μm) and a younger age (63 vs. 46 years old).

Discussion

This study implemented the OPE technique in the in vivo setting and evaluated its efficacy in characterizing corneal deformation in human eyes. Spectral analysis of the OPE-measured corneal axial motion showed strong cardiac signature. The magnitudes of in vivo corneal axial displacements measured by OPE were consistent with previous reports using other techniques. Intrasession and intersession repeatability for OPE-measured corneal parameters were both high. Calculations of corneal axial strain were demonstrated in two subjects, showing substantial difference between subjects.

Both slow and abrupt changes in amplitudes were observed in the raw cCAD signals corresponding to eye drifts and microsaccades during fixation (see Fig. 3). Drift did not affect ultrasound speckle tracking between frames acquired at a high frame rate because minimal changes occur between consecutively acquired frames. Microsaccades significantly reduced the correlation coefficients (see Fig. 3) but only had impact on small segments of the data due to their brevity (lasting 10s of ms). These results showed that high-frequency ultrasound at a high frame rate permits successful speckle tracking in most subjects despite normal involuntary fixational eye motion.

Spectral analysis and comparison of HR derived from cCAD and outputs from simultaneously recorded ECG or asynchronously recorded DCT confirmed the cardiac origin of OPE-measured corneal axial motion. This result was consistent with the findings of a strong cardiac rhythm in corneal apex motion reported in previous studies using high speed videokeratoscope[21] and A-mode ultrasound.[22]

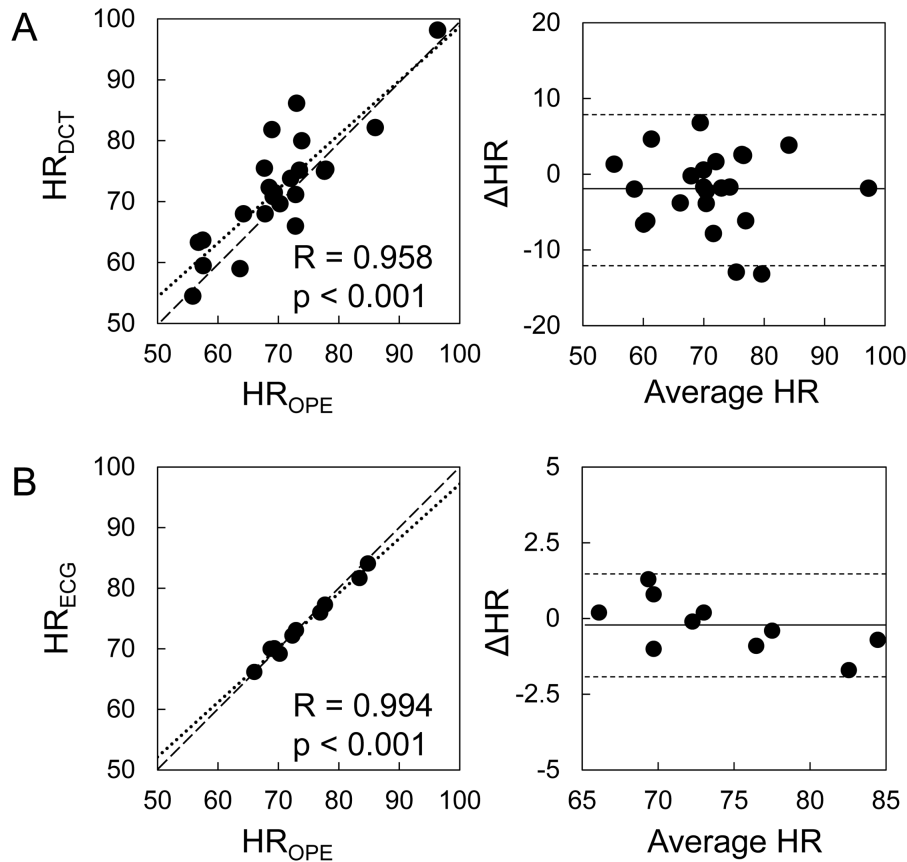The average CAD was about 47 μm in the 24 subjects measured in the present study. This magnitude

Figure 5. Scatter plots showing strong correlations between the HR calculated from OPE and the outputs of asynchronous DCT ($n = 23$) (**A**) and synchronous ECG ($n = 10$) (**B**). Bland-Altman plots show agreement between HR measured by OPE and the other techniques. OPE and DCT measurements were averaged between OD and OS.
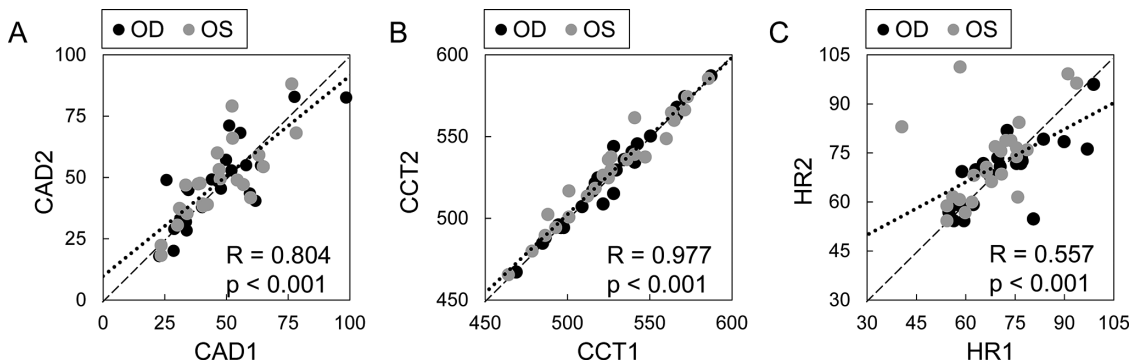

Figure 6. Intrasession repeatability of CAD (**A**), CCT (**B**), and HR (**C**) measured by OPE in 47 eyes of 24 subjects. The two repeated measurements of CAD and CCT during the same visit were strongly correlated.

was consistent with corneal apex motion measured by A-mode ultrasound[22,23] and smaller than the reported head motion which can be up to 200 μm.[5,24] As in our study, the previous studies used tight strapping of the head to a rigid head-and-chin rest, which was shown to effectively reduce heartbeat-induced head motion.[22]

A bite bar may further minimize head motion, but is inconvenient for testing a large number of subjects. The CAD was in the same order of magnitude as predicted by the Laplace's law for a thin shell of the eye's geometry and properties.[25] The range of the radial expansion would be 4 to 58 μm, if a thin shell with the human
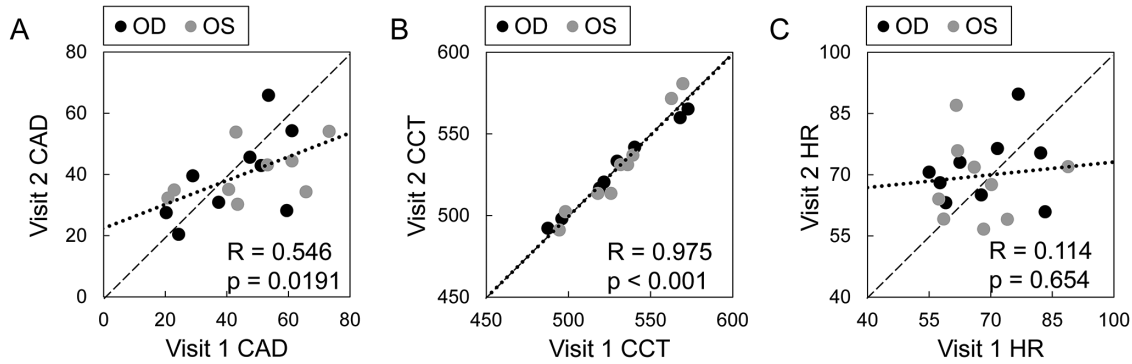
Figure 7. Intersession repeatability of CAD (**A**), CCT (**B**), and HR (**C**) measured by OPE in 18 eyes of 9 subjects. CAD and CCT were significantly correlated between visits whereas HR was not.
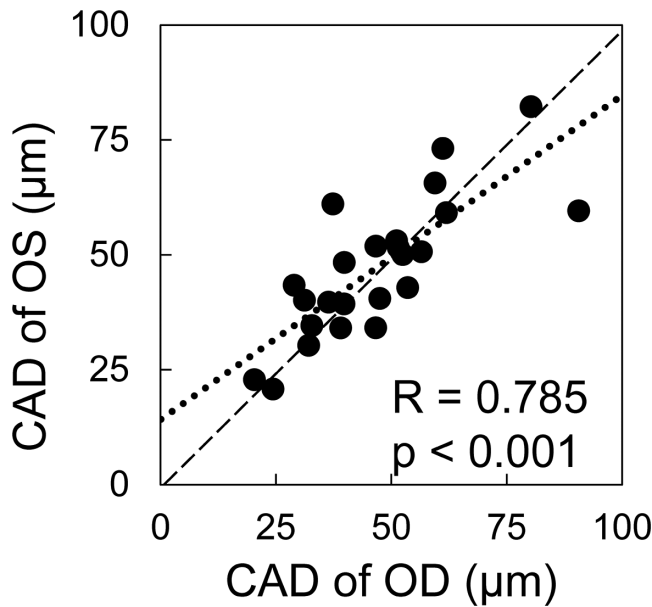

Figure 8. CAD was correlated between OD and OS ($n = 24$, all data from visit 1).

Table 2. Intrasession ($n = 24$ Subjects) and Intersession ($n = 9$ Subjects) Repeatability for OPE and DCT Parameters

	OPE			DCT		
Intrasession	CAD	CCT	HR_{OPE}	IOP	OPA	HR_{DCT}
OD	0.75	0.96	0.66	0.80	0.53	0.36
OS	0.70	0.98	0.43	0.76	0.78	0.75
Combined	0.72	0.97	0.53	0.78	0.64	0.46
Intersession						
OD	0.78	0.99	0.57	0.70	0.77	−0.07
OS	0.66	0.99	0.34	0.67	0.80	0.61
Combined	0.71	0.98	0.45	0.71	0.78	0.26

Intraclass correlation coefficients for repeated measures are listed (ICC < 0.4: poor; 0.4–0.59: fair; 0.6–0.74: good; and > 0.75: excellent agreement).

eye's thickness (0.5–1.0 mm), curvature (7.8–12 mm), and modulus (1–3 MPa) were to be inflated with the pressure of the average ocular pulse (i.e. 3 mm Hg). In the current study, CAD exhibited a substantial variance across subjects ranging from 17.9 to 98.5 µm. It is unclear which factors contributed to the intersubject variance, but CAD is at least affected by both OPA and corneal properties (modulus, thickness, and curvature) as predicted by Laplace's law, although the eye is much more complex biomechanically and hemodynamically. In the present study, we did not find significant correlations between CAD and IOP, OPA, or CCT, likely due to the limited sample size. It is also noted that CAD was not precisely repeated from heartbeat to heartbeat within a given measurement (see Fig. 2B). This variance was likely caused by fluctuations in OPA or pulsatile ocular blood flow volume from heartbeat to heartbeat.

The intrasession repeatability of OPE measurements was very high for CAD and CCT, and moderate for HR (see Fig. 6). This suggested that the high-frequency ultrasound method captured a consistent 2D cross-section of the cornea and the speckle tracking calculations yielded consistent estimates of corneal motion during repeated measurements. Interestingly, HR repeatability was lower in both OPE and DCT measurements. This is possibly due to the innate HR variability well-documented in healthy humans because only several heart beats were sampled in each measurement.[26] In addition to interocular symmetry in CCT, IOP, and OPA, which has been reported previously,[27–29] we also found a high interocular symmetry for CAD (see Fig. 8) suggesting that biomechanical characteristics are likely similar between the two eyes of the same individual.
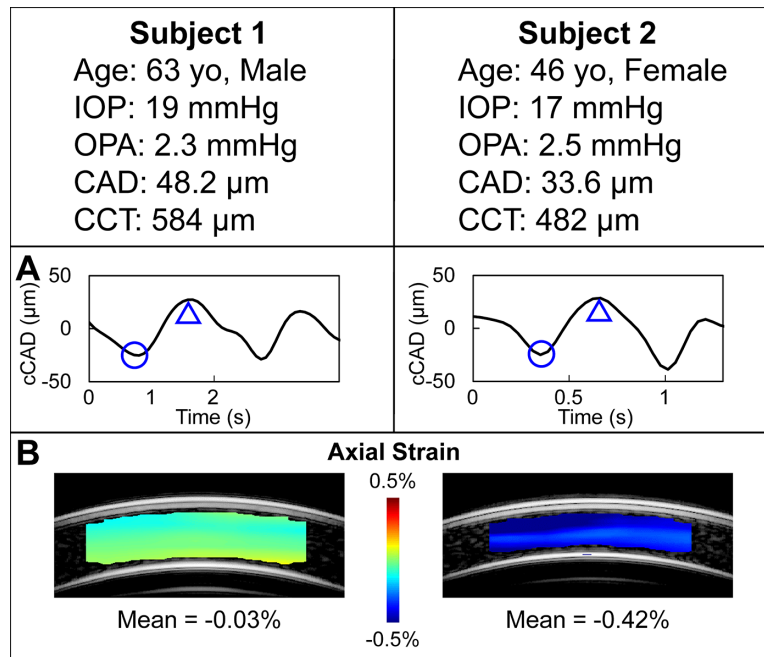
Figure 9. Corneal axial displacement and strain from two subjects of similar IOP and OPA. The bandpass-filtered cCAD over the cycles of interest are shown in (**A**). The trough (*circle*) and peak (*triangle*) of one cycle were selected from each curve to identify the two frames for axial displacement calculation using ultrasound speckle tracking. Corneal axial strains (**B**) were substantially different (−0.03% vs −0.42%, 14 folds) between the two subjects, which may be due to different structural and biomechanical properties of the corneas.

In 18 eyes with repeated visits over 6 to 10 months, OPE-measured CCT showed no change ($R = 0.98$, ICC = 0.98) and CAD was also significantly correlated and had good intrasession agreement ($R = 0.55$, ICC = 0.71). CCT was reported to not change over longer periods of time in previous reports.[30,31] This result suggested that the OPE technique was able to register a similar scanning plane during repeated visits. There was no correlation in HR_{OPE} between visits, and this was corroborated with no correlation in HR_{DCT} between visits. IOP and OPA, however, were found to be significantly correlated and showed good to excellent agreement between visits ($R = 0.65$ and 0.72, ICC = 0.64 and 0.78, respectively). Our previous ex vivo study showed that changes in IOP and OPA resulted in significant changes in OPE-measured corneal responses to simulated ocular pulses, whereas changes in cycle frequency (the HR equivalent) did not.[3] Similarly, the current intersession repeatability data suggested that the OPE-measured corneal motion remained largely unchanged when IOP and OPA were not significantly changed between visits despite variations in HR. This supported the notion that ocular pulse induced corneal motion is largely an elastic response (HR-independent) rather than a viscoelastic (HR-dependent) response.[3] Previous studies showed that IOP was correlated with diastolic and systolic blood pressure,[32] whereas OPA was not correlated with

systemic blood pressures, although it was correlated with IOP.[33] It will be of interest to evaluate the potential correlations between cardiovascular parameters, such as the blood pressure and OPE-measured cornea motion.

Corneal strains were calculated in two subjects approximately matched for IOP and OPA. Both corneas showed compressive strains between local trough and peak CAD in one cycle. The magnitude of the CAS was over 10 times different between the two eyes (−0.42% vs. −0.03%). This difference in strain may be attributed to CCT[34] or corneal modulus, which may be higher in the older subjects.[35] The in vivo CAS seen in the two eyes was in the same order of magnitude as the ocular pulse induced axial strains measured in ex vivo human donor eyes (average strain = 0.11%, n = 5, simulated diastolic IOP = 15 mm Hg, OPA = 3 mm Hg).[3] These results indicate that the in vivo corneal strain calculations are feasible despite the possible presence of residual head motion. Studies are ongoing to develop algorithms for accurate and robust strain calculations, and one challenge is the identification of time points between which strains should be calculated within each cycle in the absence of in vivo dynamic IOP recordings. Quantification of the strain map may potentially provide a diagnostic tool for keratoconus because the cone region may exhibit larger strains than the surrounding tissue, as predicted by

the mechanical weakening in the cone. However, when comparing across patients, the overall strain magnitude may not necessarily correlate with intrinsic tissue stiffness (i.e. modulus) because factors other than modulus, such as IOP, OPA, and CCT, may all affect the measured strain. Our future studies will aim to develop stiffness indices that normalize load or derive modulus values based on inverse analysis. For example, we have previously developed an "ocular pulse stiffness index (OPSI)," which takes into consideration the loading at which the OPA strains are measured.[2] We can also build computational models of the anterior eye and use inverse finite element analysis to derive modulus by matching the experimentally measured displacements and/or strains with model prediction. The computational models can incorporate the measured CAD and CAS, along with IOP, OPA, CCT, and corneal curvature, which are all measurable in vivo, to derive biomechanical properties (i.e. modulus).

Three important considerations for the successful translation of the OPE technique to in vivo are summarized below. First, we designed an acoustic coupling system consisting of solid gel (alginate), cellulose membrane, and liquid gel (GenTeal), which effectively transmits ultrasound signals without loss between the ultrasound probe and the cornea (see Fig. 1). This design avoids direct contact between the probe and the eye, which not only improves patient safety but also eliminates mechanical loading between the probe and the eye. Second, the antivibration table was useful in removing building vibration noise in the direction perpendicular to the horizontal scanning. Building vibrations could introduce significant out-of-plane motion and negatively impact tracking. Third, the acoustic power necessary for producing strong corneal speckle signals was within safety guidelines.[36] The spatially and temporally averaged (SPTA) power output of the ultrasound transducer in the focal zone I_{SPTA} was 11 mW/cm^2 at 100% power, which is within the US Food and Drug Administration (FDA) limit for ultrasound exposure of ocular tissues ($I_{SPTA} <$ 17 mW/cm^2). The mechanical index (MI) was lower than 0.4 at full power (FDA's guideline: MI < 0.23). We only used 10% power to ensure both I_{SPTA} and MI were well below the safety guideline. It is noted that the eye was exposed to acoustic energy for about 15 seconds for each measurement, and the total time for completing 3 repeated measurements in both eyes was about 10 minutes.

Various techniques and methods have been investigated toward the goal of characterizing corneal biomechanical properties in vivo, because these properties are important for understanding and diagnosing multiple ocular pathophysiologies.[37–39] For example, high-speed Scheimpflug imaging has been used to measure corneal responses to an air puff.[40,41] Optical coherence elastography (OCE) has been used to measure corneal displacements induced by a compression plate[42] or acoustic radiation force.[43] OCE has also been investigated to map corneal displacements to simulated heartbeat pulsation in ex vivo porcine eyes[44] or quasistatic increase of IOP in human donor eyes.[45] Brillouin microscopy has been used to derive local aggregate modulus that corresponds to the Brillouin frequency shift.[46] A-mode ultrasound has been used to measure corneal apex motion whose spectral characteristics (e.g. first and third harmonics) were found to change with age or glaucoma,[47] possibly correlating with corneal modulus.[48,49] The OPE method presented in this work can generate spatiotemporal quantifications of corneal displacements and strains in response to the ocular pulse, which will allow us to analyze both spectral and spatial characteristics of that response and potentially integrate the advantages of the approaches described above.

High-frequency ultrasound has a few limitations. First, the spatial resolution of high-frequency ultrasound is not as high as optical methods, such as optical coherence tomography (OCT). The 50-MHz probe we used has an axial resolution of 30 μm and a lateral resolution of 75 μm. However, despite the lower image resolution, the OPE method can achieve an axial displacement sensitivity at 10s of nanometers,[2,50] approaching that of OCEs (a few to 10s of nanometers or better with advanced systems).[44,51] During data acquisition, the corneal stroma was placed between 4.5 and 5 mm depth to ensure that it falls within the elevational and the lateral focus of the transducer. The larger image thickness of the Vevo2100 system (i.e. 155 μm) also presents an advantage for consistently tracking an imaging plane in the presence of involuntary eye motion. Second, ultrasound at 50-MHz does not penetrate through the eye lids and the patient needs to keep the eye open during OPE measurements. Although the probe only makes indirect contact with the cornea through a layer of eye-lubricating gel, this is less convenient than noncontact optical methods. Patient discomfort was minimized by applying anesthetic eye drops in both eyes, and none of the enrolled patients in this study reported pain or irritation during or after the OPE measurements.

In summary, we demonstrated the feasibility and repeatability of high-frequency ultrasound elastography for noninvasive in vivo measurement of corneal biomechanical responses to the intrinsic ocular pulse. The intrasession and intersession repeatability were both high, suggesting a robust in vivo implementation of the technique to measuring the human eye.

Combined with in vivo measurements of IOP and OPA, the OPE method may offer a useful tool for clinical biomechanical evaluations of the cornea.

Acknowledgments

References

1. Kaufmann C, Bachmann LM, Robert YC, Thiel MA. Ocular pulse amplitude in healthy subjects as measured by dynamic contour tonometry. *Arch Ophthalmol*. 2006;124(8):1104–1104.

2. Pavlatos E, Chen H, Clayson K, Pan X, Liu J. Imaging corneal biomechanical responses to ocular pulse using high-frequency ultrasound. *IEEE Trans Med Imaging*. 2018;37(2):663–670.

3. Clayson K, Pavlatos E, Pan X, Sandwisch T, Ma Y, Liu J. Ocular pulse elastography: Imaging corneal biomechanical responses to simulated ocular pulse using ultrasound. *Transl Vis Sci Technol*. 2020;9(1):5.

4. Kenneth C, Tannen B. *Eye Movement Basics for the Clinician*. First. St. Louis, MO: Mosby; 1995.

5. Kasprzak HT, Iskander DR. Ultrasonic measurement of fine head movements in a standard ophthalmic headrest. *IEEE Trans Instrum Meas*. 2010;48(1):164–170.

6. Ma Y, Pavlatos E, Clayson K, et al. Mechanical deformation of human optic nerve head and peripapillary tissue in response to acute IOP elevation. *Invest Ophthalmol Vis Sci*. 2019;60:913–920.

7. Meek KM, Tuft SJ, Huang Y, et al. Changes in collagen orientation and distribution in keratoconus corneas. *Investig Ophthalmol Vis Sci*. 2005;46(6):1948–1956.

8. Andreassen TT, Hjorth Simonsen A, Oxlund H. Biomechanical properties of keratoconus and normal corneas. *Exp Eye Res*. 1980;31(4):435–441.

9. Congdon NG, Broman AT, Bandeen-Roche K, Grover D, Quigley HA. Central corneal thickness and corneal hysteresis associated with glaucoma damage. *Am J Ophthalmol*. 2006;141(5):P868–P875.

10. Liu J, He X. Corneal stiffness affects IOP elevation during rapid volume change in the eye. *Investig Ophthalmol Vis Sci*. 2009;50(5):2224–2229.

11. Kotecha A. What biomechanical properties of the cornea are relevant for the clinician? *Surv Ophthalmol*. 2007;52(6):S109–S114.

12. Ruberti JW, Sinha Roy A, Roberts CJ. Corneal biomechanics and biomaterials. *Annu Rev Biomed Eng*. 2011;13(1):269–295.

13. Kling S, Hafezi F. Corneal biomechanics – a review. *Ophthalmic Physiol Opt*. 2017;37(3):240–252.

14. Esporcatte LPG, Salomão MQ, Lopes BT, et al. Biomechanical diagnostics of the cornea. *Eye Vis (Lond)*. 2020;7(1):9.

15. Perez BC, Pavlatos E, Morris H, et al. Mapping 3D strains with ultrasound speckle tracking: method validation and initial results in porcine scleral inflation. *Ann Biomed Eng*. 2016;44(7):2302–2312.

16. Tang J, Liu J. Ultrasonic measurement of scleral cross-sectional strains during elevations of intraocular pressure: method validation and initial results in posterior porcine sclera. *J Biomech Eng*. 2012;134(9):91007.

17. Beaton L, Mazzaferri J, Lalonde F, et al. Non-invasive measurement of choroidal volume change and ocular rigidity through automated segmentation of high-speed OCT imaging. *Biomed Opt Express*. 2015;6(5):1694.

18. Kallel F, Ophir J. A least-squares strain estimator for elastography. *Ultrason Imaging*. 1997;19(3):195–208.

19. Shrout PE, Fleiss JL. Intraclass correlations: uses in assessing rater reliability. *Psychol Bull*. 1979;86(2):420–428.

20. Cicchetti DV. Guidelines, criteria, and rules of thumb for evaluating normed and standardized assessment instruments in psychology. *Psychol Assess*. 1994;6(4):284–290.

21. Robert Iskander D, Kasprzak HT. Dynamics in longitudinal eye movements and corneal shape. *Ophthalmic Physiol Opt*. 2006;26(6):572–579.

22. Kowalska MA, Kasprzak HT, Iskander DR, Danielewska M, Mas D. Ultrasonic in vivo measurement of ocular surface expansion. *IEEE Trans Biomed Eng*. 2011;58(3):674–680.

23. Danielewska ME, Kicińska AK, Placek MM, Lewczuk K, Rękas M. Changes in spectral parameters of corneal pulse following canaloplasty. *Graefe's Arch Clin Exp Ophthalmol*. 2019;257(11):2449–2459.

24. de Kinkelder R, Kalkman J, Faber DJ, et al. Heartbeat-induced axial motion artifacts in

optical coherence tomography measurements of the retina. *Investig Ophthalmol Vis Sci*. 2011;52(6):3908–3913.

25. Chung CW, Girard MJA, Jan NJ, Sigal IA. Use and misuse of Laplace's law in ophthalmology. *Investig Ophthalmol Vis Sci*. 2016;57(1):236–245.

26. Acharya UR, Joseph KP, Kannathal N, Lim CM, Suri JS. Heart rate variability: a review. *Med Biol Eng Comput*. 2006;44(12):1031–1051.

27. Myrowitz EH, Kouzis AC, O'Brien TP. High interocular corneal symmetry in average simulated keratometry, central corneal thickness, and posterior elevation. *Optom Vis Sci*. 2005;82(5):428–431.

28. Li Y, Bao FJ. Interocular symmetry analysis of bilateral eyes. *J Med Eng Technol*. 2014;38(4):179–187.

29. Perkins ES. The ocular pulse. *Curr Eye Res*. 1981;1(1):19–23.

30. Muir KW, Duncan L, Enyedi LB, Stinnett SS, Freedman SF. Central corneal thickness in children: stability over time. *Am J Ophthalmol*. 2006;141(5):955–957.

31. Brandt JD, Gordon MO, Beiser JA, Lin SC, Alexander MY, Kass MA. Changes in central corneal thickness over time. The Ocular Hypertension Treatment Study. *Ophthalmology*. 2008;115(9):1550–1556.

32. Klein BEK, Klein R, Knudtson MD. Intraocular pressure and systemic blood pressure: longitudinal perspective: the Beaver Dam Eye Study. *Br J Ophthalmol*. 2005;89(3):284–287.

33. Grieshaber MC, Katamay R, Gugleta K, Kochkorov A, Flammer J, Orgül S. Relationship between ocular pulse amplitude and systemic blood pressure measurements. *Acta Ophthalmol*. 2009;87(3):329–334.

34. Chen MC, Lee N, Bourla N, Hamilton DR. Corneal biomechanical measurements before and after laser in situ keratomileusis. *J Cataract Refract Surg*. 2008;34(11):1886–1891.

35. Elsheikh A, Wang D, Brown M, Rama P, Campanelli M, Pye D. Assessment of corneal biomechanical properties and their variation with age. *Curr Eye Res*. 2007;32(1):11–19.

36. Silverman RH, Lizzi FL, Ursea BG, et al. Safety levels for exposure of cornea and lens to very high-frequency ultrasound. *J Ultrasound Med*. 2001;20(9):979–986.

37. Vellara HR, Patel D V. Biomechanical properties of the keratoconic cornea: a review. *Clin Exp Optom*. 2015;98(1):31–38.

38. Medeiros FA, Meira-Freitas D, Lisboa R, Kuang TM, Zangwill LM, Weinreb RN. Corneal hysteresis as a risk factor for glaucoma progression: a prospective longitudinal study. *Ophthalmology*. 2013;120(8):1533–1540.

39. Clayson K, Pan X, Pavlatos E, et al. Corneoscleral stiffening increases IOP spike magnitudes during rapid microvolumetric change in the eye. *Exp Eye Res*. 2017;165:29–34.

40. Vinciguerra R, Ambrósio R, Elsheikh A, et al. Detection of keratoconus with a new biomechanical index. *J Refract Surg*. 2016;31(12):803–810.

41. Ambrósio R, Ramos I, Luz A, et al. Dynamic ultra high speed Scheimpflug imaging for assessing corneal biomechanical properties. *Rev Bras Oftalmol*. 2013;72(2):99–102.

42. De Stefano VS, Ford MR, Seven I, Dupps WJ. Depth-dependent corneal biomechanical properties in normal and keratoconic subjects by optical coherence elastography. *Transl Vis Sci Technol*. 2020;9(7):4.

43. Li Y, Zhu J, Chen JJ, et al. Simultaneously imaging and quantifying in vivo mechanical properties of crystalline lens and cornea using optical coherence elastography with acoustic radiation force excitation. *APL Photonics*. 2019;4(10):106104–106110.

44. Nair A, Singh M, Aglyamov SR, Larin K V. Heartbeat OCE: corneal biomechanical response to simulated heartbeat pulsation measured by optical coherence elastography. *J Biomed Opt*. 2020;25(05):1.

45. Kling S, Torres-Netto EA, Spiru B, Sekundo W, Hafezi F. Quasi-static optical coherence elastography to characterize human corneal biomechanical properties. *Invest Ophthalmol Vis Sci*. 2020;61(6):29.

46. Scarcelli G, Besner S, Pineda R, Kalout P, Yun SH. In vivo biomechanical mapping of normal and keratoconus corneas. *JAMA Ophthalmol*. 2015;133(4):180–482.

47. Danielewska ME, Krzyzanowska-Berkowska P, Iskander DR. Glaucomatous and age-related changes in corneal pulsation shape. The ocular dicrotism. *PLoS One*. 2014;9(7):e102814.

48. Rogala MM, Danielewska ME, Antończyk A, et al. In-vivo corneal pulsation in relation to in-vivo intraocular pressure and corneal biomechanics assessed in-vitro. An animal pilot study. *Exp Eye Res*. 2017;162:27–36.

49. Rogala MM, Lewandowski D, Detyna J, Antończyk A, Danielewska ME. Corneal

pulsation and biomechanics during induced ocular pulse. An ex-vivo pilot study. *PLoS One*. 2020;15(2):e0228920.

50. Akyildiz AC, Hansen HHG, Nieuwstadt HA, et al. A framework for local mechanical characterization of atherosclerotic plaques: combination of ultrasound displacement imaging and inverse finite element analysis. *Ann Biomed Eng*. 2016;44(4):968–979.

51. Li Y, Moon S, Chen JJ, Zhu Z, Chen Z. Ultrahigh-sensitive optical coherence elastography. *Light Sci Appl*. 2020;9:58.

Supplementary Material

Supplement Video S1. The B-mode video (slowed to half speed) from one eye was synchronized with the corneal lateral displacement calculated from ultrasound speckle tracking. Microsaccades (quick eye movement lasting 10s of ms) coincided with abrupt changes in corneal displacements (*red segments* in the curve). Drifts (slower, gradual eye movements) were observed throughout the recording.